Palladium nanoparticles supported on boron oxides (B_xO_y) incorporated graphene sheets for enhanced formic acid oxidation

Yanan Xie [a], Juan Wang [a], Xing Huang [b*], Bowen Luo [a], Weizhen Yu [a], Lidong Shao [a*]

[a] Shanghai Key Laboratory of Materials Protection and Advanced Materials in Electric Power, Shanghai University of Electric Power, Shanghai 200090, China

[b] Department of Inorganic Chemistry, Fritz-Haber Institute of the Max Planck Society, Faradayweg 4-6, 14195 Berlin, Germany

Corresponding Authors

[*] Correspondence to: lidong.shao@shiep.edu.cn (L.D.S.)

[*] Correspondence to: xinghuang@fhi-berlin.mpg.de (X.H.)

Keywords

HCOOH electrooxidation; B_xO_y-incorporated; graphene sheets; electron transfer

Abstract

In the present study, Pd nanoparticles supported on boron oxides (B_xO_y) incorporated holey graphene sheets (Pd/BG) and unmodified holey graphene sheets (Pd/G) are prepared through heating treatment and impregnation method. The synthesized Pd/BG and Pd/G are characterized by Raman, XRD, TEM, XPS and applied as electrocatalysts for formic acid electrooxidation. In contrast to the sluggish activity toward HCOOH oxidation on Pd/G, Pd/BG shows obviously enhanced catalytic activity and stability. We propose that the smaller particle size and electron transfer caused by B_xO_y incorporation contribute to the improved electrocatalytic performance.

Introduction

Recently, direct formic acid fuel cells (DFAFCs) have been recognized as a promising candidate for portable power sources with high power density and energy efficiency. The fuel of DFAFCs, formic acid, is a type of superior feedstock with many advantages such as non-toxicity, safer storage and transportation than H_2, lower crossover flux through Nafion than ethanol, and fast oxidation kinetics [1,2,3]. Pt- and Pd-based catalysts are the two main types of anode catalysts used in DFAFCs. Pd is cheaper and more abundant than Pt. Furthermore, it is recognized that Pd catalysts exhibit higher activity toward formic acid oxidation than Pt catalysts [4]. For these reasons, Pd-based catalysts have been well studied.

Many efforts have been made to synthesize various novel Pd-based catalysts, such as alloying with transition metal [5], forming different nanostructures [6] and

supported catalysts [7]. Among these ingenious approaches, Pd nanoparticles supported on carbon materials exhibit excellent performance because of their large specific area and improved Pd utilization [8]. Graphene is a single layer of sp^2-bonded carbon atoms that are densely packed into a two-dimensional honeycomb lattice with the advantages of a large specific surface area, superior electrical conductivity, and many other intriguing electronic properties [9]. Furthermore, chemical doping with heteroatoms can tailor the structure and electronic properties of graphene-based materials [10-12]. Boron is regarded as a good substitute for carbon atoms and it can act as a p-type dopant [13]. To date, boron-doped graphene structures have been investigated as electrode materials in oxygen reduction reactions, supercapacitors, and photocatalysts [14]. However, there are few reports of doped graphene-based sheets as support materials for the loading of any metal to facilitate HCOOH oxidation.

In light of the above consideration, here we prepare Pd supported on B_xO_y incorporated holey graphene sheets (Pd/BG). It shows higher catalytic activity and stability than Pd supported on unmodified graphene sheets (Pd/G). The incorporation of B_xO_y changes particle size and the electronic properties of Pd nanoparticles to facilitate the HCOOH oxidation.

Material and methods

A colloidal dispersion of graphene oxide synthesized from Hummers method [15] was desiccated by lyophilization. Subsequently, heating was applied under vacuum at 300°C (G). Further heating was conducted at 1000°C under a He/H_2 atmosphere with boron oxide (B_2O_3), the acquired material was washed by 90 ℃ distilled water for

three times and dried under vacuum at 60ºC to obtain B_xO_y-incorporated holey graphene sheets (BG). 30 μL $Pd(NO_3)_2$ (Sigma-Aldrich) were added to the 10 mL of water containing 50 mg G or BG under sonication. Then the solvent was removed by lyophilization. Finally the collected powder was annealed in a tube furnace at 250°C under a He/H_2 atmosphere to fabricate Pd/G and Pd/BG catalysts with 3 wt.% Pd loading.

The morphology of the samples were investigated by an FEI aberration-corrected Titan 80-300 transmission electron microscope in both TEM and STEM modes, and the X-ray diffraction (XRD) patterns were obtained using a Bruker D8 Advance X-ray diffractometer with Cu-Kα radiation. Raman spectra of these samples were examined by a HORIBA Scientific LabRAM HR Evolution Raman spectrometer with an incident laser beam of 633 nm. Surface electronic states were analyzed by X-ray photoelectron spectroscopy (XPS, PHI 5000 Versaprobe) with Al Kα excitation.

Results and discussion

Fig. 1. shows the schematic representation of the preparation of supports G and BG. First, graphene oxide is disordered with greater interlayer spacing after lyophlization treatment. Then the interlayer spacing becomes small after vacuum treatment. Last, partial oxygen functionalities are replaced by B_xO_y through 1000℃ annealing treatment with B_2O_3.

Fig. 2. (a) shows the typical TEM image of Pd/BG with the inset of the size distribution diagram of Pd nanoparticles, the average size of Pd is around 4.5 ± 0.2 nm. Energy-filtered transmission electron microscopy (EFTEM)-energy-dispersive

X-ray spectroscopy (EDX) element mapping distributions of C、O and B are presented in Fig. 2. (b)、(c) and (d), respectively, indicating the homogeneous distribution of O and B in the Pd/BG. Fig. 2. (e) shows the Pd dispersion status on BG with the inset of a high-resolution TEM image of a Pd nanoparticle. Fig. 2. (f) shows the STEM image of Pd/BG which maintain membrane structure after the incorporation of B_xO_y.

The XRD patterns of (a) Pd/G and (b) Pd/BG catalysts are shown in Fig. 3. (A). In the spectrum of Pd/G, the peaks at 2θ = 26.30° and 43.01° of Pd/G correspond to C(002) and C(101), respectively (JCPDS, 41-1487). The peaks at 40.00°, 46.55°, 68.01°, and 81.97° are assigned to the (111), (200), (220), and (311) crystal faces of the face-centered cubic crystalline structure of Pd (JCPDS, 46-1043). In the spectrum of Pd/BG, the distinct difference in the diffraction intensity is noteworthy: adding B_xO_y causes the intensity of Pd-related peaks to be lower and softer, indicating a smaller Pd particle size in Pd/BG than in Pd/G [16]. Further, the intensity of the carbon peaks also decreased, indicating that the crystallinity of the support decreased with the addition of B_xO_y. The average size of palladium nanoparticles (d) for Pd/G was calculated by the Scherrer's equation (Eq.1) [16] for the (111) peak after background subtraction:

$$d= k\lambda/(\beta\cos\theta) \quad (1)$$

where k is a coefficient, generally taken as 0.9, λ is wavelength of X-ray radiation(1.5418Å), β is the full width at half maximum (FWHM) measured in radians, and θ is the angle measured for the position of palladium peaks. The average size of Pd particles for Pd/G is calculated to be 15.6 ± 0.2 nm, which is bigger than

the average size of Pd for Pd/BG demonstrated by the size distribution in Fig. 2. (a).

Fig. 3. (B) shows the Raman spectra of (a) Pd/BG and (b) Pd/G. Both catalysts show two distinct bands, the G band at around 1580 cm^{-1} and the D band at around 1350 cm^{-1}. Generally, the value of I_D/I_G is used to determine the degree of disorder of carbon materials [17]. The intense G band in Pd/G and Pd/BG indicates that both catalysts maintain graphitic structure after the vacuum and 1000°C annealing treatment with boron oxide. However, the slightly higher I_D/I_G value (1.06) for Pd/BG in comparison with that for Pd/G (0.84) suggests that there appears more planner lattice defects after the 1000°C annealing treatment. The change may due to the cutting effect induced by heating treatment to make graphene sheets become smaller structures with more defects at edges.

X-ray photoelectron spectroscopy (XPS) is employed to reveal the surface composition and electronic structure of Pd/BG. In the B 1s spectra of Pd/BG (Fig. 4A), the presence of the B 1s signal (186 eV-196 eV) indicates that B element has been introduced into Pd/BG. Cermignani et al. [18] and Jacques et al. [19] assigned the peaks at 190.0±0.3 and 192.0±0.2eV to partially oxidized boron atoms such as BC_2O and BCO_2, respectively. In our work, the B 1s XPS spectrum shows peak at 192.1 eV in Fig. 4A indicating the presence of boron oxides (B_xO_y) which is incorporated in the networks of holey graphene sheets.

Fig. 4B shows the Pd 3d XPS spectra of Pd/G and Pd/BG. In the fitted Pd 3d core-level spectra of Pd/BG (spectrum a in Fig. 4B), the Pd $3d_{5/2}$ peak at 336.04 eV and the Pd $3d_{3/2}$ peak at 341.29 eV are assigned to Pd^0, while the $3d_{5/2}$ peak at 337.56

eV and the Pd $3d_{3/2}$ peak at 342.78 eV are assigned to $Pd^{II}O$ species [20,21]. In the spectra of Pd/G (spectrum b in Fig. 4B), Pd $3d_{5/2}$ (335.57eV), Pd $3d_{3/2}$ (340.83eV) and Pd $3d_{5/2}$ (337.21eV), Pd $3d_{3/2}$ (342.46eV) can be assigned to Pd^0 and $Pd^{II}O$ species, respectively. The peak appearing at highest binding energy values in Pd/G and Pd/BG are contributed to divalent polynuclear Pd-hydroxo complexes caused by the incompletely reduced precursor Pd salts or reprecipitated species in the reacted samples [22]. Notably, the binding energy values of Pd^0 and $Pd^{II}O$ species in catalysts Pd/BG shift 0.46 eV and 0.33 eV more positively compared to Pd/G, respectively. These significant changes can be ascribed to the strong interaction between Pd nanoparticles and B_xO_y incorporated supports. When Pd nanoparticles interact with BG, Pd would donate electrons to BG resulting in the decreased electrons density of Pd nanoparticles in Pd/BG.

Fig. 5A shows the cyclic voltammograms (CVs) of formic acid electrooxidation in a deaerated 0.5 M HCOOH + 0.5 M H_2SO_4 electrolyte solution on the Pd/BG and Pd/G electrodes at a scan rate of 50 mV s^{-1}. During the catalytic tests, we found that Pd/G displayed no catalytic activity towards HCOOH electrooxidation. Vacuum treatment pulled graphene sheets close while removing the adsorped water, but treated G still contains a high percentage of oxygen atoms and functional groups in the holey structures. Pd dispersed on functional groups enriched support with low electric conductivity (high defects in graphitic units) results in the sluggishness of Pd/G towards formic acid electrooxidation. On the contrary, the anodic peak of HCOOH oxidation on the Pd/BG electrode was located at 0.13 V, and the corresponding mass

activity was 557.95 A g^{-1}.

To further estimate the electrocatalytic stability of the catalysts for HCOOH oxidation, chronoamperometry tests in deaerated 0.5 M H_2SO_4 + 0.5 M HCOOH at a constant potential of 0.15 V were conducted for 3600 s. As shown in Fig. 5B, during the entire process, Pd/G possessed no activity for formic acid oxidation. In the case of Pd/BG, in the first 1000 s, the mass activity of Pd/BG was 70.70 A g^{-1}. In the next 1000 s, the mass activity of Pd/BG was 52.44 A g^{-1}, which maintains 10.2% of its initial mass activity (taken at 20s to avoid the contribution of the double-layer discharge and hydrogen adsorption) [23]. These observation shows that Pd/BG possess a relatively good stability towards formic acid electrooxidation.

When Pd salt precursors interact with BG, the active sites caused by B_xO_y incorporation will work as anchoring points to fix salt precursors. After metal ions coordinated with BG, hydrolysis was applied to crystallize the precursors nucleated on the B_xO_y incorporated graphene sheets to form nanocrystals [24,25]. Meanwhile, the interaction between Pd and B_xO_y modified graphene sheets can restrain the growth of Pd particles during reduction process. The lower 3d electron density of Pd makes the adsorption strength of formate intermediate weaker, so the surface (COOH)ads coverage is reduced [20], which is beneficial to formic acid electrooxidation through the direct pathway.

Conclusions

In conclusion, we demonstrate a facile way to prepare B_xO_y incorporated holey graphene sheets (BG) through vacuum and heating treatment of graphene oxide. Pd/G

and Pd/BG are fabricated using a simple impregnation method and then applied in HCOOH oxidation as anode catalysts. Compared to sluggish electrochemical performance of Pd/G, the enhanced catalytic activity and stability of Pd/BG towards HCOOH oxidation in 0.5 M H_2SO_4 + 0.5 M HCOOH are observed. Surface analyses show that the smaller particle size of Pd and electron transfer caused by B_xO_y incorporation graphene sheets contributes to the improved electrocatalytic performance.

Acknowledgement

This work is supported by the National Natural Science Foundation of China (21403137).

References

[1] U.B. Demirci, Direct liquid-feed fuel cells: Thermodynamic and environmental

concerns, J. Power Sources 169 (2007) 239-246.

[2] Y.M. Zhu, S.Y. Ha, R.I. Masel, High power density direct formic acid fuel cells, J. Power Sources 130 (2004) 8-14.

[3] N.V. Rees, R.G. Compton, Sustainable energy: a review of formic acid electrochemical fuel cells, J. Solid State Electrochem. 15 (2011) 2095-2100.

[4] Z.L. Liu, L. Hong, M.P. Tham, T.H. Lim, H.X. Jiang, Nanostructured Pt/C and Pd/C catalysts for direct formic acid fuel cells, J. Power Sources 161 (2006) 831-835.

[5] X. Wang, Y.W. Tang, Y. Gao, T.H. Lu, Carbon-supported Pd–Ir catalyst as anodic catalyst in direct formic acid fuel cell, J. Power Sources 175 (2008) 784-788.

[6] Y.Z. Lu, W. Chen, Nanoneedle-covered Pd-Ag nanotubes: high electrocatalytic activity for formic acid oxidation, J. Phys. Chem. C. 114 (2010) 21190-21200.

[7] G.Z. Hu, F. Nitze, H.R. Barzegar, T. Sharifi, A. Mikołajczuk, C.W. Tai, A Borodzinski, T. Wågberg, Palladium nanocrystals supported on helical carbon nanofibers for highly efficient electro-oxidation of formic acid, methanol and ethanol in alkaline electrolytes, J. Power Sources 209 (2012) 236-242.

[8] J. Yang, C.G. Tian, L. Wang, H.G. Fu, An effective strategy for small-sized and highly-dispersed palladium nanoparticles supported on graphene with excellent performance for formic acid oxidation, J. Mater. Chem. 21 (2011) 3384-3390.

[9] A.K. Geim, K.S. Novoselov, The rise of graphene, Nature materials 6 (2007) 183-191.

[10] M.M. Liu, R.Z. Zhang, W. Chen, Graphene-supported nanoelectrocatalysts for fuel cells: synthesis, properties, and applications, Chem. Rev. 114 (2014) 5117-5160.

[11] S.X. Liang, C. Hao, Y.T. Shi, The Power of Single-Atom Catalysis, ChemCatChem. 7 (2015) 2559-2567.

[12] W. Zhang, W.T. Zheng, Single Atom Excels as the Smallest Functional Material, Adv. Funct. Mater. 26 (2016) 2988–2993.

[13] Y.B. Tang, L.C. Yin, Y. Yang, X.H. Bo, Y.L. Cao, H.E. Wang, W.J. Zhang, I. Bello, S.T. Lee, H.M. Cheng, C.S. Lee, Tunable band gaps and p-type transport properties of boron-doped graphenes by controllable ion doping using reactive microwave plasma, Acs Nano. 6 (2012) 1970-1978.

[14] M.Y. Xing, W.Z. Fang, X.L. Yang, B.Z. Tian, J.L. Zhang, Highly-dispersed boron-doped graphene nanoribbons with enhanced conductibility and photocatalysis, Chem. Commun. 50 (2014) 6637-6640.

[15] W.S. Hummers, R.E. Offeman, Preparation of graphitic oxide, J. Am. Chem. Soc. 80 (1958) 1339.

[16] M.M. Demir, M.A. Gulgun, Y.A. Menceloglu, et al., Palladium nanoparticles by electrospinning from poly (acrylonitrile-co-acrylic acid)-$PdCl_2$ solutions, Relations between preparation conditions, particle size, and catalytic activity, Macromolecules 37 (2004) 1787-1792.

[17] M.M. Lucchese, F. Stavale, E.H. Martins Ferreira, C. Vilani, M.V.O. Moutinho, Rodrigo B. Capaz, C.A. Achete, A. Jorio, Quantifying ion-induced defects and Raman relaxation length in graphene, Carbon 48 (2010) 1592-1597.

[18] W. Cermignani, T.E. Paulson, C. Onneby, C.G. Pantano, Synthesis and characterization of boron-doped carbons, Carbon 33 (1995) 367-374.

[19] S. Jacques, A. Guette, X. Bourrat, F. Langlais, C. Guimon, C. Labrugere, LPCVD and characterization of boron-containing pyrocarbon materials, Carbon 34 (1996) 1135-1143.

[20] W.J. Zhou, J.Y. Lee, Particle size effects in Pd-catalyzed electrooxidation of formic acid, J. Phys. Chem. C. 112(2008) 3789-3793.

[21] H. Meng, S.H. Sun, J.P. Masse, J.P. Dolelet, Electrosynthesis of Pd single-crystal nanothorns and their application in the oxidation of formic acid, Cham. Mater. 20 (2008) 6998-7002.

[22] H.F. Wang, W.E. Kaden, R. Dowler, M. Sterrer, H.J. Freund, Model oxide-supported metal catalysts–comparison of ultrahigh vacuum and solution based preparation of Pd nanoparticles on a single-crystalline oxide substrate, Phys. Chem. Chem. Phys. 14 (2014) 11525-11533.

[23] Y. Chen, Y.M. Zhou, Y.W. Tang, T.H. Lu, Electrocatalytic properties of carbon-supported Pt-Ru catalysts with the high alloying degree for formic acid electrooxidation, J. Power Sources 195 (2010) 4129-4134.

[24] R.N. d'Alnoncourt, M. Friedrich, E. Kunkes, D. Rosenthal, F. Girgsdies, B.S. Zhang, L.D. Shao, M. Schuster, M. Behrens, R, Schlögl, Strong metal–support interactions between palladium and iron oxide and their effect on CO oxidation, Journal of Catalysis 317 (2014) 220-228.

[25] X.T. Li, C.B. McAuley, S.A.I. Whitby, K. Tschulik, L.D. Shao, R.G. Compton, Single Nanoparticle Voltammetry: Contact Modulation of the Mediated Current, Angew. Chem. Int. Ed. 55 (2016) 4296 –4299.

Figures

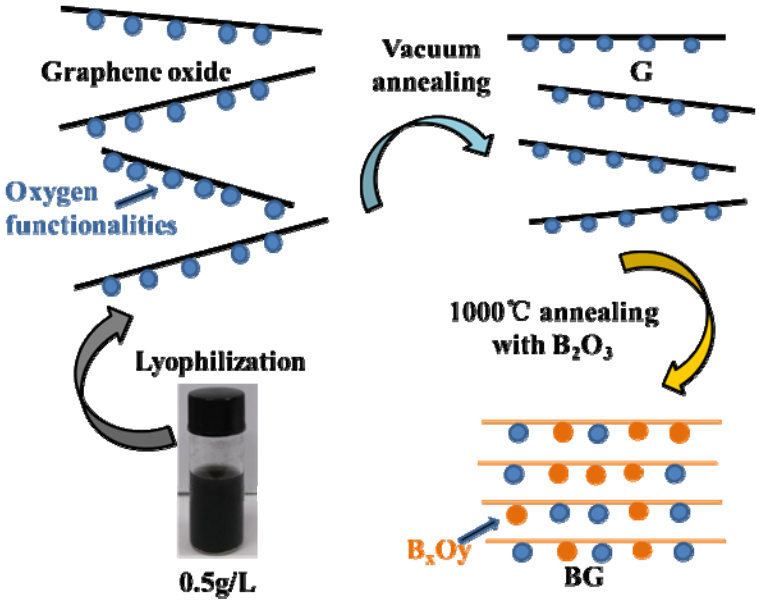

Fig. 1

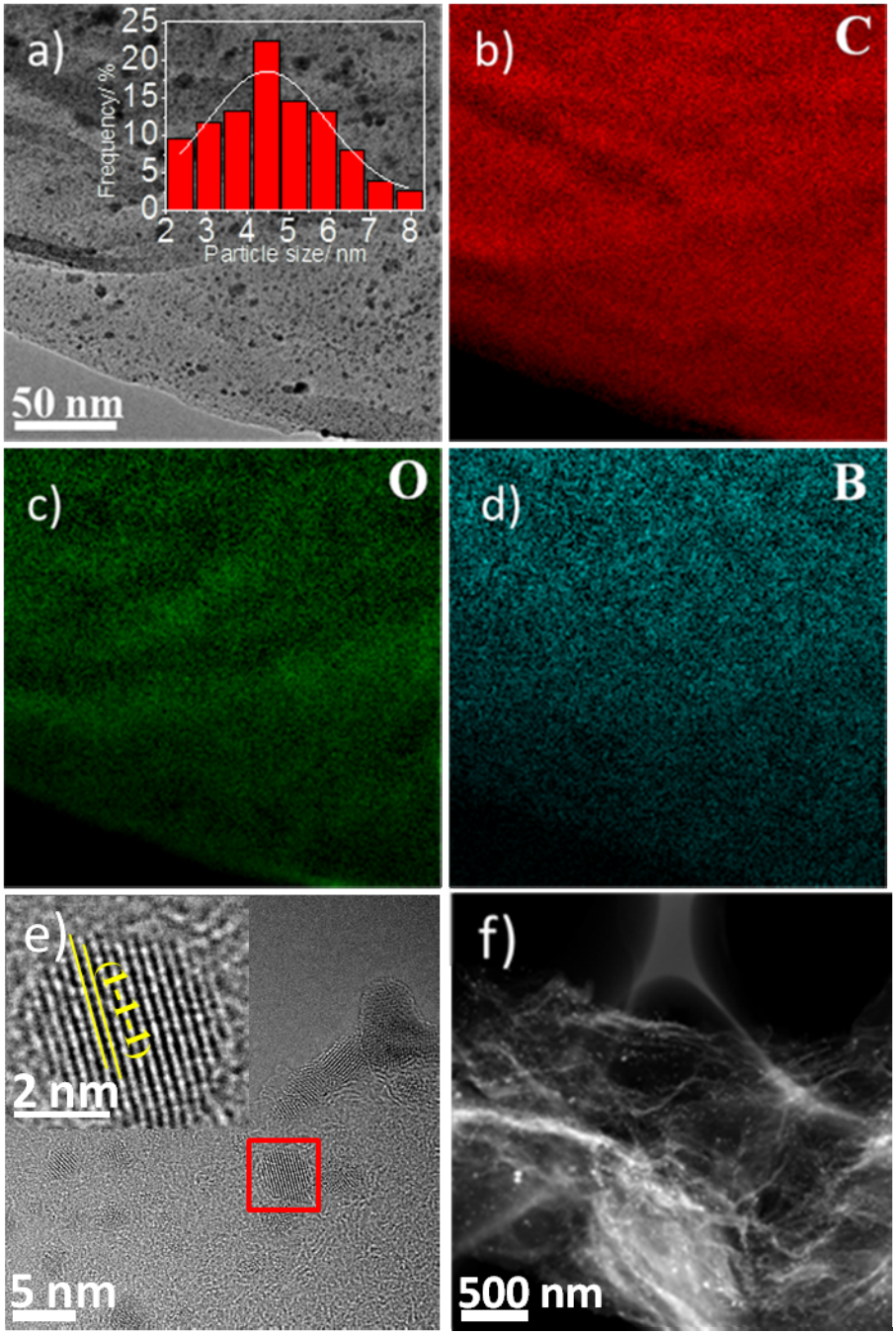
a)
Frequency/ %
25
20
15
10
5
0
2 3 4 5 6 7 8
Particle size/ nm
50 nm
b)
C
c)
O
d)
B
e)
0.1 nm
2 nm
5 nm
f)
500 nm

Fig. 2

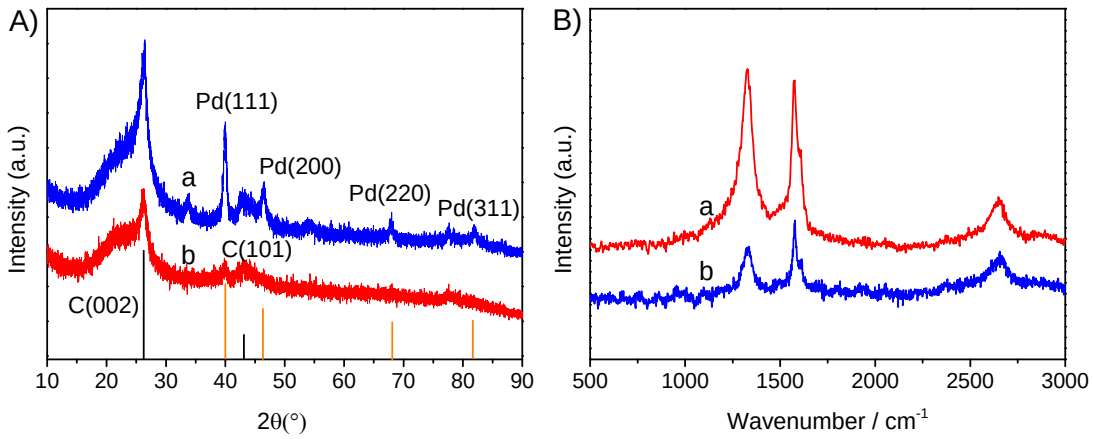
A)
Intensity (a.u.)
Pd(111)
Pd(200)
Pd(220)
Pd(311)
a
b
C(101)
C(002)
10
20
30
40
50
60
70
80
90
2θ(°)
B)
Intensity (a.u.)
a
b
500
1000
1500
2000
2500
3000
Wavenumber / cm-1

Fig. 3

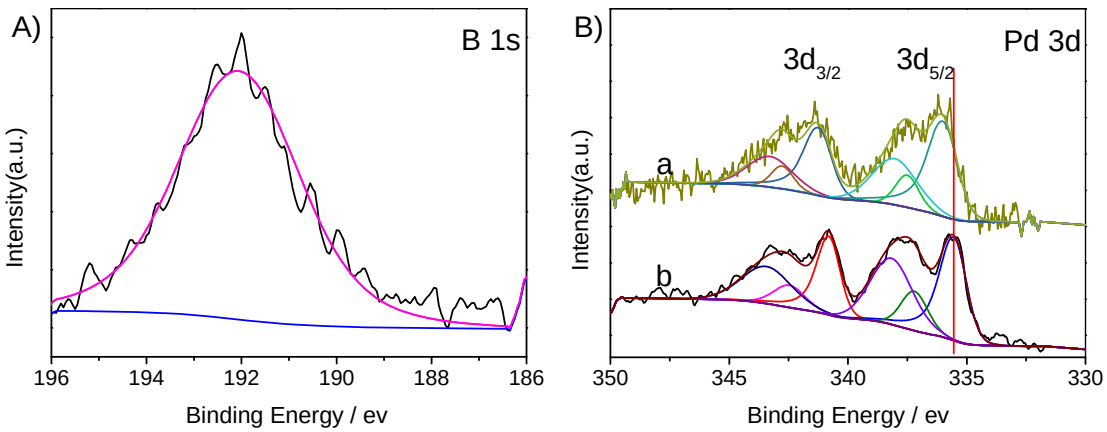
A)
B 1s
Intensity(a.u.)
196
194
192
190
188
186
Binding Energy / ev
B)
Pd 3d
3d3/2
3d5/2
a
b
Intensity(a.u.)
350
345
340
335
330
Binding Energy / ev

Fig. 4

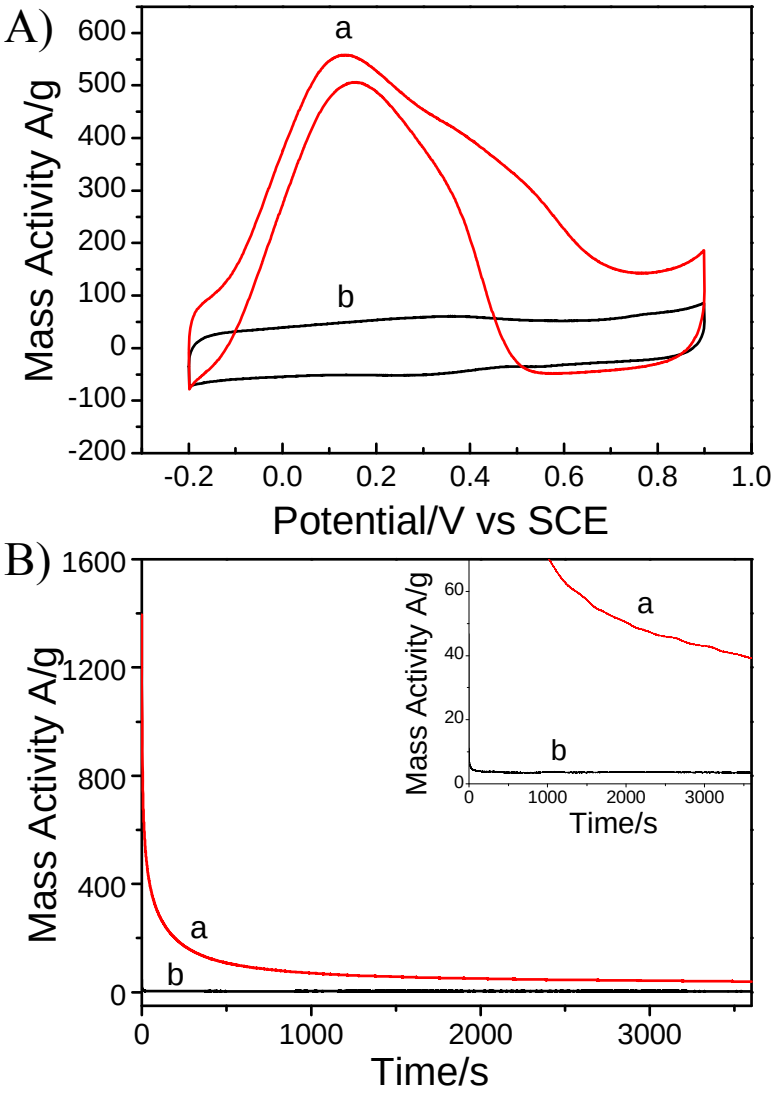
A)
Mass Activity A/g
Potential/V vs SCE
a
b
B)
Mass Activity A/g
Time/s
a
b

Fig. 5

Figure Captions

Fig. 1. Schematic representation of the preparation of G and BG.

Fig. 2. (a) TEM image of Pd/BG with an inset of Pd size distribution. (b)、(c) and (d) EFTEM-EDX element mapping distributions of C、O and B. (e) TEM image of Pd nanoparticles supported on BG with an inset of a HRTEM image of a Pd nanoparticle. (f) STEM image of Pd/BG.

Fig. 3. A) XRD patterns of (a) Pd/G and (b) Pd/BG. B) Raman spectra of (a) Pd/BG and (b) Pd/G.

Fig. 4. (A) XPS spectrum of Pd/BG in B1s region. (B) XPS spectrum of (a) Pd/BG and (b) Pd/G in Pd 3d regions.

Fig. 5. A) Cyclic voltammograms of formic acid oxidation on (a) Pd/BG and (b) Pd/G catalysts in deaerated 0.5 M H_2SO_4 + 0.5 M HCOOH solution at a scan rate of 50 mV s^{-1}. B) Chronoamperometry curves of (a) Pd/BG and (b) Pd/G catalysts in 0.5 M H_2SO_4 + 0.5 M HCOOH solution at a constant potential of 150 mV.